Dielectric Stack Filters for *Ex Situ* and *In Situ* UV Optical-Fiber Probe Raman Spectroscopic Measurements

CALUM H. MUNRO, VASIL PAJCINI, and SANFORD A. ASHER*

University of Pittsburgh, Department of Chemistry, Pittsburgh, Pennsylvania 15260

Dielectric stack interference filters can be used in conjunction with a high-throughput single-stage spectrograph to facilitate the measurement of high signal-to-noise (S/N) ultraviolet (UV) Raman spectra with 228.9-nm and 244-nm excitation wavelengths. Placed between the sample and the spectrograph, these filters reflect Rayleigh scattering while transmitting Stokes-shifted Raman scattering. We have measured UV Raman bands from solid, highly scattering samples down to a 290-cm^{-1} shift from the Rayleigh line. The high throughput of the filtered single-stage spectrograph enables the measurement of UV Raman spectra from photo-labile samples, including DNA and the energetic materials pentaerythritol tetranitrate (PETN) and trinitrotoluene (TNT), with sufficiently low excitation powers and short accumulation times to minimize photo-alteration. High S/N UV preresonance and resonance Raman are obtained for PETN and TNT within 1 s, indicating the possible application of UV Raman spectroscopy as a rapid, highly selective screening methodology for the detection of trace levels of contraband explosives. Furthermore, the incorporation of these dielectric filters within a UV optical-fiber Raman probe head provides simultaneous Rayleigh rejection and removal of background silica Raman scattering. With the use of a 244-nm UV optical-fiber probe, we measured Raman spectra from 100 nM to 10 μM concentrations of polycyclic aromatic hydrocarbon (PAH) in water, even in the presence of an equimolar concentration of the visible fluorophore rhodamine 6G (R6G). Thus, we demonstrate the potential of UV Raman optical-fiber probes for minimally invasive *in situ* real-time monitoring at low analyte concentrations and within environments in which fluorescence backgrounds would prevent measurements with visible Raman optical-fiber probes.

Index Headings: **UV Raman spectroscopy; Instrumentation; Dielectric UV filters; Optical fibers; PETN; TNT; DNA; PAH.**

INTRODUCTION

The advantages of ultraviolet (UV) Raman (UVR) and UV-resonance Raman (UVRR) spectroscopies have become well established over the past decade,[1–26] provoking the development and application of new "Raman friendly" continuous-wave (CW) UV-excitation sources and efficient multichannel UV detectors.[27–31]

In addition to efficient excitation and detection, the successful measurement of a UV Raman spectrum requires the effective rejection of the dominant Rayleigh scattering from the Raman-scattered photons. While the advantages of single spectrograph dispersion, with holographic notch filters for the rejection of Rayleigh scattering, have been well demonstrated for visible Raman spectroscopy and imaging,[32–39] holographic notch filters are not available for operation in the UV region. Thus, UV Raman measurements still normally require notoriously inefficient triple-stage monochromators or spectrographs for the rejection of Rayleigh scattering and stray light. Between 200 nm and 270 nm, <1–3% of the Raman-scattered photons entering the entrance slit of a standard triple-stage UV Raman spectrograph are transferred to the detector.

We recently demonstrated the application of dielectric stack filters for Rayleigh rejection at 244 nm in a high-efficiency UVR microspectrometer employing single-spectrograph dispersion.[40] These dielectric stack filters comprise multiple quarter-wave, optically thick alternating layers of high- and low-index refractory metal oxides that were evaporated under high vacuum. Incident light is subject to interference between filter layers and will be reflected or transmitted depending on wavelength. Stack filters, with a design wavelength corresponding to that of a UVR-excitation source, reflect Rayleigh scattering while transmitting Stokes-shifted Raman-scattered light.

We report here the properties of dielectric stack filters with design wavelengths of 244 and 228.9 nm, including their transmission angular dependence and temperature stability, and demonstrate their potential to facilitate the application of UVR spectroscopy as a powerful analytical technique. We demonstrate the ability to measure UVR bands of solid and absorbing solid samples close to the Rayleigh line with a single spectrograph. We exploit the high throughput efficiency of a filtered single-stage compared with a triple-stage spectrograph to measure high signal-to-noise (S/N) UVR spectra from photo-labile samples using low excitation powers and short accumulation times to minimize photo-alteration. We also demonstrate the incorporation of dielectric filters within an optical-fiber probe head both for Rayleigh rejection and for the removal of background silica Raman signals and illustrate the potential advantages of this UVR optical-fiber probe.

EXPERIMENTAL

Dielectric stack filters with design wavelengths of 228.9 and 244 nm were custom-made by Omega Optical Inc. Transmission measurements were made by using a Perkin–Elmer Lambda 9 UV-visible near-infrared (near-IR) spectrophotometer with a resolution of 0.1 nm. A quartz polarization scrambler or a custom UV calcite Glan–Thompson prism was used in front of the filters for unpolarized and polarized light measurements, respectively.

Ultraviolet Raman spectra were excited with a Coherent Innova 300 intracavity frequency-doubled argon-ion laser system. Raman scattering was imaged into a Spex 1701, 0.75-m single monochromator (*f*/6.8) equipped with a 3600-groove/mm holographic grating and an EG&G PARC 1456 blue-intensified photodiode array and an optical multichannel analyzer. All measurements were

Received 9 December 1996; accepted 31 March 1997.
* Author to whom correspondence should be sent.

0003-7028/97/5111-1722$2.00/0

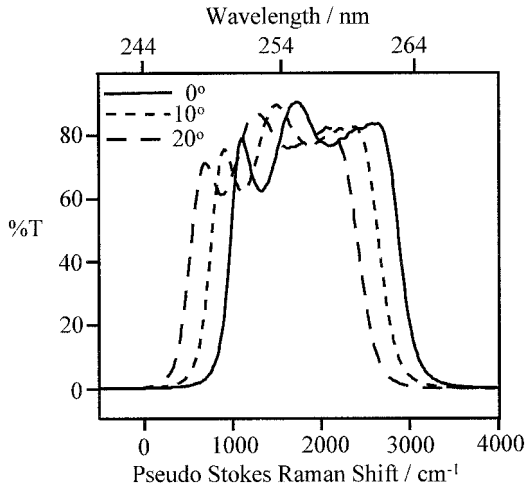

FIG. 1. Transmittance vs. wavelength and pseudo Stokes Raman shift for a dielectric filter with a design wavelength of 244 nm. Unpolarized light was incident at angles of 0°, 10°, and 20° from the filter normal.

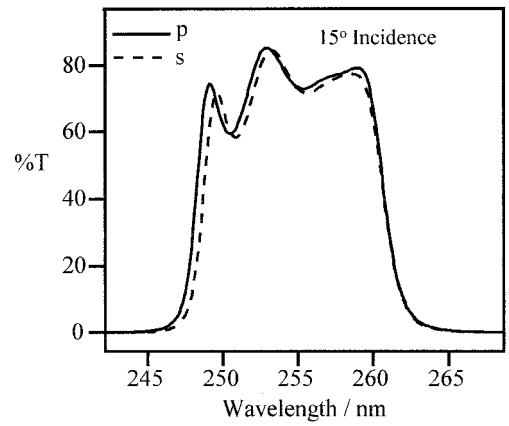

FIG. 2. Transmittance of *p*- and *s*-polarized light vs. wavelength for a dielectric filter with a design wavelength of 244 nm with light incident at 15° from the filter normal.

made with an excitation power of 3 mW, an accumulation time of 10 × 1 s, and a spectrograph entrance slit width of 100 μm unless otherwise stated.

The six-around-one optical-fiber probe was custom-made by CIC Photonics, Inc. Polyimide-coated, high-OH optical fibers used in the construction of the filtered optical-fiber probe head were from Fiberguide Industries. Calf thymus DNA, rhodamine 6G (R6G), and pyrene were from Calbiochem Corp., Eastman Kodak Co., and Lab Services, respectively, and were used without further purification. The energetic materials, pentaerythritol tetranitrate (PETN) and trinitrotoluene (TNT), were supplied from the Naval Surface Warfare Center, Indian Head Division, and Mason & Hanger-Silas Mason Co. Inc., on arrangement by the Federal Aviation Administration (FAA).

The DNA base concentration was determined from absorption measurements by using a nucleic acid absorptivity at 260 nm of 6550 M^{-1} cm^{-1}.[24] DNA films (100–150 μm thick) were prepared by room-temperature (~ 294 K) evaporation of an aqueous solution of calf thymus DNA (base concentration, 6.7 mM; ~ 50 μL) on suprasil substrates. Final film concentrations of ~ 32 and ~ 24 mM DNA were also determined by UV-absorption spectrophotometry.

RESULTS AND DISCUSSION

We have examined the optical characteristics of two dielectric stack filters designed for the rejection of Rayleigh scattering in Raman measurements performed by using the 244-nm and 228.9-nm lines from a frequency-doubled argon-ion laser. The 244-nm stack was produced by the ion-assisted deposition of approximately quarter-wave-thick layers comprising silica (SiO_2) and hafnia (HfO_2), while the 228.9-nm stack was produced by using scandium oxide (Sc_2O_3) in place of hafnia.

Transmission Characteristics. Figure 1 shows the angular dependence of the transmittance spectrum for a dielectric filter with a design wavelength of 244 nm vs. wavelength and pseudo Stokes Raman shift. Here we define pseudo Stokes Raman shift as the wavenumber shift from that of the design wavelength. Transmittance measurements were performed with unpolarized light. The 244-nm dielectric stack filter exhibits an angle dependence: The band-pass shifts toward shorter wavelengths as the angle of incidence (the angle between the incident ray and the filter surface normal) increases. With normal incidence, the filter has an optical density (OD) of 3.37 at 244 nm; a maximum transmittance of 91% at ~ 255 nm (~ 1740 cm^{-1} pseudo Raman shift); and a Raman "working window", where the bandpass transmittance is >3%, of ~ 248–265 nm (660–3250 cm^{-1} pseudo Raman shift). With an angle of incidence of 20°, the OD at 244 nm is reduced slightly to 3.18, the maximum transmittance is reduced to 87%, and the bandpass working window is blue-shifted to between 245.5 and 261.5 nm (250–2740 cm^{-1} pseudo Raman shift).

The optimum filter operating angle for UVR measurements with 244-nm excitation is determined primarily by the desired working window. However, the intensity of Rayleigh scattering must also be considered, especially when one is examining highly scattering samples. Maximum Rayleigh rejection is achieved with normal incidence, but the Raman working window will be limited to wavenumber shifts of >660 cm^{-1}. For the measurement of Raman bands close to the Rayleigh line, the filter can be angle-tuned to blue-shift the working window. For highly scattering solid or absorbing samples, this blue shift may result in a rising Rayleigh tail underlying the low wavenumber-shifted Raman bands and stray-light artifacts. Figure 2 shows the polarization dependence of the dielectric filter transmittance for light incident at 15° from the normal. The position of the short wavelength band edge blue shifts ~ 25 cm^{-1} with *s*-polarized light and red shifts ~ 15 cm^{-1} with *p*-polarized light when compared to that observed with unpolarized light. Thus, the polarization of the incident light is another important consideration when one is angle tuning the spectral window.

Figure 3 shows a plot of percentage transmittance vs. wavelength and pseudo Stokes Raman shift for a dielectric filter with a design wavelength of 228.9 nm. This 228.9-nm filter has a maximum OD at 228.9 nm of 2.78 and exhibits angle and polarization dependencies similar to those described in detail for the 244-nm filter.

Environmental Stability. Immunity from environ-

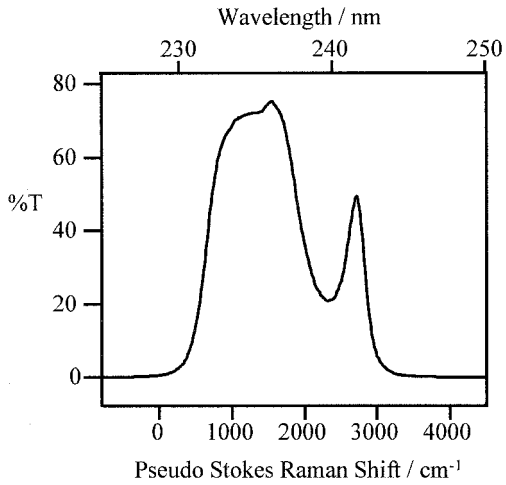

FIG. 3. Transmittance vs. wavelength and pseudo Stokes Raman shift for a dielectric filter with a design wavelength of 228.9 nm with unpolarized light incident along the filter normal.

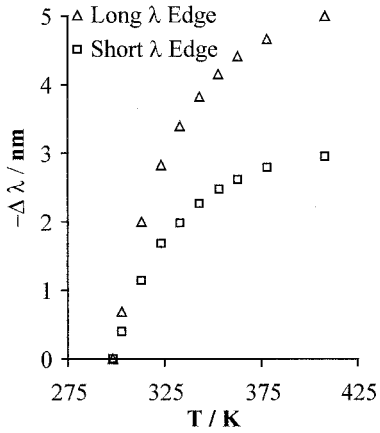

FIG. 4. Wavelength shift ($\Delta\lambda$) of the short- and long-wavelength edges of the 244-nm filter with temperature. Band-edge positions were measured at the 50% transmittance levels.

mental effects such as temperature and humidity is a highly desirable property of any optical component, especially if the instruments are used in the field. Bandpass dielectric stack filters, produced by ion-assisted deposition, have previously shown stability of their optical properties with changing temperature and humidity.[41]

We measured the optical characteristics of the filter with a design wavelength of 244 nm at room temperature (294 ± 1 K) through 10 sequential temperature cycles from room temperature to >500 K to <277 K. The relative humidity remained at ~ 30% throughout the 10 temperature cycles. There was no statistically significant change for the filter band edge positions, maximum transmittance, or OD at room temperature. Standard deviations of 0.055 and 0.058 nm for 10 replicate measurements of the short- and long-wavelength band edge positions at the 50% transmittance levels are within the experimental errors for replicate room temperature measurements of the filter in the absence of temperature cycling.

The refractory metal oxide filter remains stable through repeated cycling to high temperatures without observable alteration of room-temperature optical characteristics. However, Fig. 4 shows the temperature dependence of the short- and long-wavelength band edge positions at 50% transmittance levels. Although the filter is not degraded by operation at high temperature, it does exhibit significant temperature tuning of the bandpass. The bandpass blue shifts with increasing temperature (Fig. 4). The blue shift is not linear with increasing temperature: The rate of shift decreases at higher temperatures. The rate of blue shift for the long-wavelength band edge is 1.689× larger than for the short-wavelength edge, resulting in a narrowing of the bandpass. Furthermore, the slope of the long- and short-wavelength band edges determined between the 10 and 60% transmittance levels changes with temperature. At 400 K, the slope of the long-wavelength edge increases (~ 9%) compared with that at 300 K. However, the slope of the short-wavelength edge decreases (~ 11%) at 400 K with respect to 300 K. Thus, while the long-wavelength cutoff sharpens with increasing temperature, the short-wavelength cutoff becomes less sharp. A sharp short-wavelength cutoff is desirable for Raman–Stokes measurements; thus room-temperature operation of the dielectric filter is preferential.

In addition, we measured the optical characteristics of the filter with a design wavelength of 244 nm at room temperature (294 ± 1 K) and normal incidence with humidity levels of 0 and 100%. The stack filter exhibits an insignificant red shift of ~ 0.12 nm with an increase in relative humidity from 0 to 100%. This wavelength shift may be attributed to water absorption by the SiO_2 layers. This small quantity of absorbed water can be readily removed by heating the filter *in vacuo,* without observable filter degradation.

The 228.9-nm filter exhibits environmental dependencies similar to those described for the 244-nm filter: A reversible and reproducible nonlinear blue shift and narrowing of the bandpass occur with increasing temperature, while a negligible red shift follows an increase in relative humidity from 0 to 100%.

Application to Raman Measurements. We utilized dielectric filters with design wavelengths of 244 and 228.9 nm for UVR measurements of highly scattering solid and absorbing samples using a single-stage spectrograph equipped with multichannel detector. The filters were incorporated within the optical path of the scattered light between the sample and the spectrograph to reject radiation scattered at the Rayleigh wavelength while transmitting the Stokes-shifted Raman scattering.

Figure 5 shows the UVR spectra of Teflon™ measured with the use of a single spectrograph without filtering and with the use of dielectric stack filters designed for excitation with 244- and 228.9-nm light. Teflon™ is a highly scattering solid with a number of low-energy Raman bands that cannot be readily measured with a conventional single spectrograph but instead requires a lossy triple-stage spectrograph to provide sufficient Rayleigh rejection to discriminate these bands from the intense Rayleigh tail and stray-light background. The unfiltered scattering spectrum is dominated by the Rayleigh tail (Fig. 5a). However, when the dielectric stack filters are positioned between the Teflon™ sample and the entrance slit of the spectrograph, the effective rejection of the dominant Rayleigh scattering enables the low-energy Raman

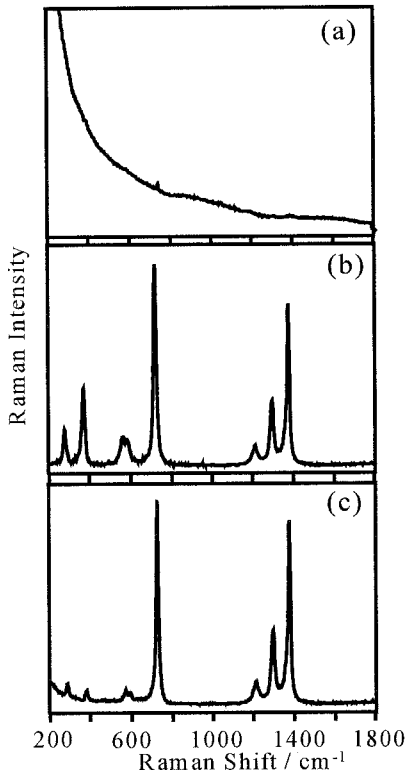

FIG. 5. UVR spectrum of Teflon™ measured by using a single spectrograph with 244-nm excitation (**a**) unfiltered, (**b**) with the 244-nm dielectric filter, and (**c**) with the 228.9-nm excitation and the 228.9-nm filter. Excitation conditions: 244 or 228.9 nm; 1 mW; 10 s.

bands to be discerned easily from the background (Figs. 5b and 5c).

The high throughput efficiency of the filtered single-stage spectrograph enables the measurement of high S/N spectra with reduced accumulation times and excitation powers compared with that utilizing less efficient triple-stage spectrographs. This capability is especially advantageous for the measurement of low Raman scattering cross-section analytes or photo-labile samples. For example, Fig. 6 shows the UVRR spectrum from a ~ 100-μm-thick film of calf thymus DNA excited at 244 nm, within the broad nucleic acid $\pi^* \leftarrow \pi$ absorbance bands (236–282 nm).[42] With the use of the filtered single spectrograph with a blue-intensified multichannel detector, this high S/N spectrum could be obtained by using only 0.2 mW of 244-nm excitation and a 20-s accumulation time, thereby preventing observable photo-degradation of this photo-labile sample. The DNA UVRR spectrum is dominated by the ~ 1484-cm^{-1} band due to the overlapping bands of adenine at 1482 cm^{-1} and guanine at 1480–1485 cm^{-1}.[43,44] The broad bands at 1333 cm^{-1} and 1575 cm^{-1}, with shoulders at ~ 1315 cm^{-1} and 1610 cm^{-1}, also derive from adenine and guanine ring vibrations,[44] while the 1412-cm^{-1} band is assigned to the ring vibration of cytosine.[43] We recently demonstrated that these mild experimental conditions could be used to excite the UVRR spectrum of DNA selectively from within the macronucleus of a single living paramecium.[40]

Similarly, Fig. 7 shows the UVR spectrum from a ~ 10-μm single crystal of the energetic material PETN and from solid TNT acquired with 5 mW of 244-nm ex-

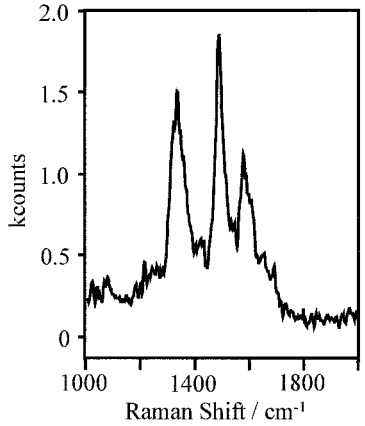

FIG. 6. UVRR spectrum of a ~ 32 mM, 100-μm-thick film of calf thymus DNA. Excitation conditions: 244 nm; 0.2 mW; 20-μm spot diameter (64 Wcm^{-2}); 20-s accumulation time.

citation focused to a 10-μm spot size and a 1-s accumulation time. The high S/N UV preresonance and resonance Raman spectra, obtained for these highly UV photo-labile materials with a short accumulation time, suggest the possibility of applying UVR spectroscopy as a rapid, highly selective screening methodology for the detection of trace levels of contraband explosives.

UV Optical-Fiber Probe. The application of incisive analytical techniques to real-time *in situ* chemical characterization is important for process control and for monitoring or screening of illicit or hazardous materials.[45,46] In addition, well-defined minimally invasive chemical monitoring schemes must be developed to allow for real-

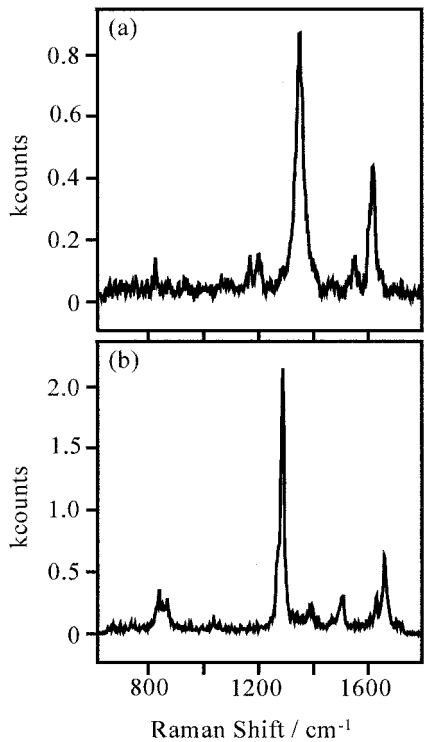

FIG. 7. UVR spectrum (**a**) from a ~ 10-μm single crystal of the energetic material PETN and (**b**) from solid TNT. Excitation conditions: 244 nm; 5 mW; 10-μm spot diameter (6.4 $kWcm^{-2}$); 1-s accumulation time.

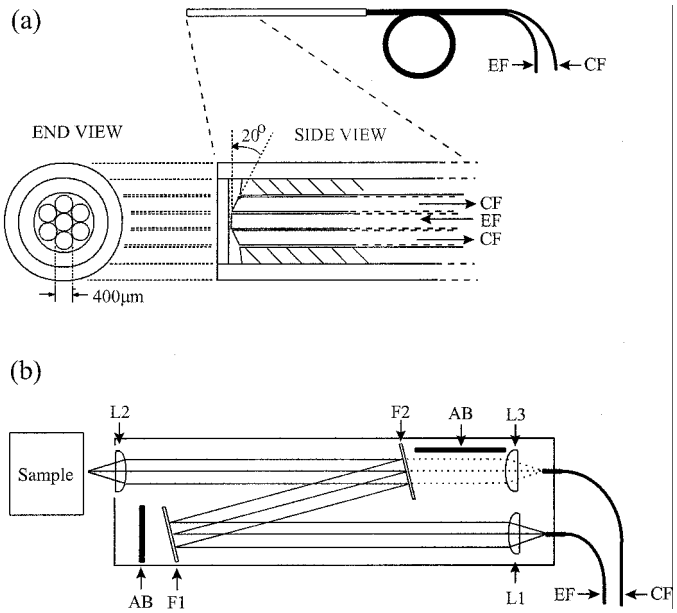

FIG. 8. Schematic of the optical layout of (**a**) an unfiltered optical-fiber probe with a six-around-one arrangement and (**b**) an optical-fiber probe head incorporating the 244-nm dielectric filters for removal of the silica background and the Rayleigh scattering. **EF**, excitation fiber; **CF**, collection fiber; **F**, filter; **L**, lens; **AB**, absorbing baffle.

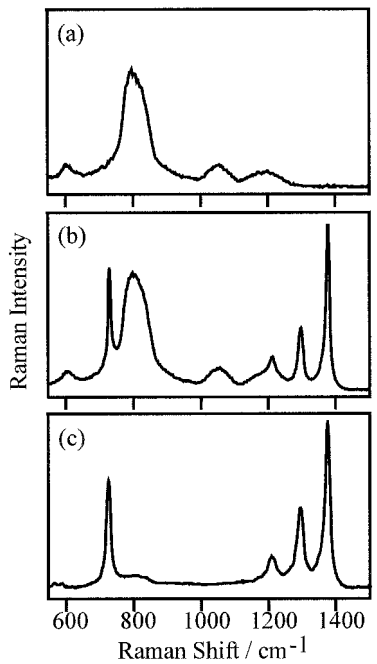

FIG. 9. UVR spectrum of (**a**) a fused-silica optical fiber, (**b**) Teflon™ measured by using an unfiltered optical-fiber probe, and (**c**) Teflon™ measured by using an optical-fiber probe incorporating dielectric filters for removal of Rayleigh scattering and the silica background. Excitation conditions: 244 nm; 1 mW; 10 s.

time, *in situ* measurements within potentially harsh environments that are not readily accessible.

Infrared and visible Raman spectroscopies have been used extensively for chemical component characterization *ex situ* or *in situ* by the use of appropriate optical-probe systems employing optical trains or fibers. Visible Raman spectroscopy has the advantage that it can be readily applied to remote sampling due to the availability of high-throughput optical-fiber probes. There have been significant recent advances in the design and application of visible Raman optical-fiber probes,[45–53] and the utility of visible Raman optical-fiber measurements is now well demonstrated.[45–50] However, in many instances, the small visible Raman cross sections and the common nuisance of fluorescence interference result in low S/N visible Raman spectra, hindering or even preventing real-time spectroscopic monitoring of real, nonpurified samples.

Ultraviolet-resonance Raman can circumvent the deficiencies of visible Raman with the ability to invoke strong resonance enhancements without fluorescence interference.[2] However, material and instrumentation limitations have greatly hindered remote UVRR optical-fiber probe measurements. One such limitation has been the inability to easily remove the interfering silica background signal generated on transmittance of the excitation source through the excitation fiber. (The excitation fiber is the optical fiber along which the excitation radiation is transmitted from the laser or equivalent excitation source to the sample, while those optical fibers that transmit the scattered radiation from the sample to the spectrograph are the collection fibers.) The removal of the silica background has been readily demonstrated with visible Raman optical-fiber probes through the incorporation of holographic or interference optics to filter the radiation exiting the excitation fiber and entering the collection fibers.[45,51–53] A similar application of the dielectric stack filters described here can facilitate the use of UV optical-fiber probes for remote Raman measurements.

Figure 8a shows a fused-silica bifurcated optical-fiber probe with a six-around-one geometry. The central excitation fiber is surrounded by six collection fibers. The collection fibers are tapered at 20° to maximize the overlap of the field of view between the collection and excitation fibers close to the tip of this unlensed fiber probe.[46] Figure 8b shows the 244-nm optical-fiber probe head that incorporates two dielectric stack filters to simultaneously remove the silica Raman background generated within the excitation fiber prior to the sample and also to reject Rayleigh scattering prior to transmittance of the sample Raman scattering through the collection fiber to the spectrograph.

The 244-nm light exiting the excitation fiber is collimated with a short-focal-length lens (**L1**). This collimated beam, which also contains the silica Raman-scattered light, is incident on the first 244-nm dielectric stack filter (**F1**) at an angle of approximately 15° from the normal. More than 99% of the 244-nm excitation radiation is reflected by this first filter toward the second filter (**F2**), while up to 75% of the silica Raman signal is transmitted. The reflected collimated beam is filtered similarly by the second filter and is focused by lens **L2** onto the sample. The scattered radiation is collected via the same lens and collimated. The collimated scattered radiation passes back to the second dielectric stack filter where the Rayleigh line is rejected before the Raman signal is launched into the collection fiber via lens **L3**. The high-OH optical fibers utilized in the filtered probe showed no observable degradation with operation at 244 nm.

Figure 9a shows the UVR spectrum of a silica fiber, while Figs. 9b and 9c show the UVR spectrum of Tef-

lon™ measured with the unfiltered six-around-one and the prototype-filtered probes, respectively. A significant silica signal is superimposed onto the Teflon™ spectrum measured with the use of the unfiltered probe (Fig. 9b). The relative intensity of the background and sample signals is dependent on the sampling distance from the end of the unfiltered probe. This dependence had been described recently by Coonen et al.[46] and will be reported in further detail with respect to this system in a future publication. The data shown here were collected at the optimum sampling distance for the reduction of the silica background signal with respect to the sample signal. The Teflon™ spectrum measured by using the probe that incorporates dielectric stack filters for the simultaneous removal of the silica Raman background signal and rejection of radiation scattered by the sample at the Rayleigh wavelength exhibits a >90% reduction in the relative intensity of the background silica spectrum compared with that of the unfiltered probe.

The use of identical plano-convex lenses **L1**, **L2**, and **L3** results in insignificant chromatic aberrations over the short-wavelength range associated with a UVR working window. Corrections for the alteration to relative band intensities resulting from these minimal chromatic aberrations and from variations in filter transmission across the Raman spectral window can be applied during corrections for the relative spectrograph and detector efficiencies.

Remote Environmental Monitoring. Polycyclic aromatic hydrocarbons (PAHs) are prevalent environmental pollutants that are known to be highly carcinogenic, either binding covalently to, or intercalating within, DNA to result in cell mutation or tumor formation.[54–56] Thus, it is important to detect and monitor low levels of these chemical species in the environment, especially in water systems. We recently showed that UVRR enabled the detection of nanomolar quantities of PAH.[57]

We demonstrate here that the superior sensitivity, selectivity, and immunity from fluorescence interference of UVRR compared with visible optical-fiber probe measurements enables the monitoring of low levels of PAH in aqueous systems. Figures 10a, 10b, and 10c show the UVRR spectra of 10 μM, 1 μM, and 100 nM pyrene in water (2 ppm, 200 ppb, and 20 ppb, respectively) measured by dipping the head of the optical-fiber probe directly into the sample solutions. The spectrum of the 100 nM (20 ppb) solution shows that the 1632-cm^{-1} pyrene band can be readily discerned from the noise with a low-excitation power (3 mW on sample) and relatively short accumulation time (200 s), illustrating the advantage of high sensitivity.

Figure 10d shows the UVR spectrum from 1 μM pyrene in a 1 μM aqueous solution of the visible fluorophore R6G. This figure clearly illustrates the major advantages of UV excitation over visible: sensitivity, selectivity, and immunity from fluorescence interference. First, selective resonance enhancement by exciting at 244 nm, within the pyrene S4 absorbance band (λ_{max} = 241.4 nm), results in a complete dominance of the spectrum by pyrene bands and no readily observable bands due to R6G (Fig. 10e). Second, UVR measurement is not compromised by the immense visible fluorescence cross section

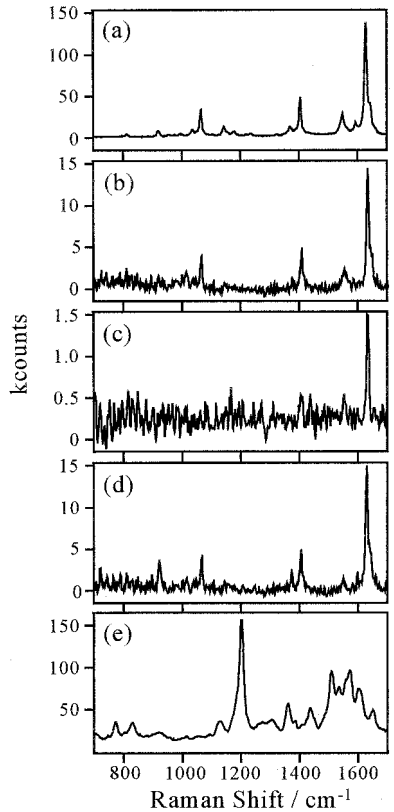

FIG. 10. UVR spectrum from (**a**) 10 μM (2 ppm), (**b**) 1 μM (200 ppb), and (**c**) 100 nM (20 ppb) pyrene in water; (**d**) 1 μM pyrene in a 1 mM aqueous solution of R6G; and (**e**) 100 μM R6G. Spectra were obtained by using a UV optical-fiber probe dipped directly into the analyte solutions. Excitation conditions: (**a–d**) 244 nm, 3 mW, 200 s; (**e**) 244 nm, 7.5 mW, 300 s.

of R6G that prevents the measurement of visible Raman spectra of R6G or other analytes.

The filtered probe utilized fused-silica optical fibers, each 2 m in length. One further consideration that has previously hindered the realization of the potential of UVR for remote monitoring is that the effective working length of UVR optical-fiber probes is limited compared with that of visible and near-IR systems: The measured transmittance of fused-silica optical fibers is 84% ± 1% for 1 m at 244 nm and decreases as the wavelength decreases (62% ± 1% for 1 m at 206.5 nm).

This apparent length limitation does not dramatically impede UVR measurements compared to visible or near-IR Raman measurements. Raman excitation light in the deep UV results in an enhancement in the scattering intensity due to the dependence of the Raman scattered radiation intensity, I_s, on the fourth power of the scattering frequency, ω_s^4($I_s = k\omega_s^4$). As a result, with equivalent excitation powers and accumulation times, the scattering intensity observed with 244-nm excitation is at least 16× greater than that observed with excitation at 488 nm, e.g. 19× greater for an aromatic ring-stretching mode with a Stokes shift of ~ 1600 cm^{-1}. Therefore, while the transmittance of optical fibers is only ~ 84% per meter at 244 nm, compared with ~ 99% at 488 nm, the inherent increase in scattering intensity with excitation at the UV wavelength is greater than the decrease that results from transmission losses through up to 16 m of fiber. Thus,

the observed scattering intensity measured by using an optical-fiber probe comprising one excitation fiber and one collection fiber of up to 8 m in length (16 m total optical fiber) would be greater with excitation at 244 nm than at 488 nm.

In addition, visible Raman measurements are often hindered by laser-induced fluorescence interference. The standard solution to this problem is to employ near-IR excitation to minimize the fluorescence background, but this red shift in excitation and thus in the Stokes-shifted Raman scattering wavelength will further reduce the scattering intensity. With the use of deep UV excitation, the high inherent scattering intensity is combined with immunity from fluorescence interference (for condensed-phase species) to result in very high S/N UVRR spectra. Furthermore, exciting within an analyte's UV absorption band results in the selective resonance enhancement of the analyte Raman scattering signal by as much as 10^8. This additional enhancement of the scattering intensity can more than compensate for further signal losses observed with optical fiber probes >8 m in length.

CONCLUSION

Dielectric stack interference filters can be used in conjunction with a high-throughput single-stage spectrograph to facilitate the measurement of high S/N UVR spectra with 228.9- and 244-nm excitation wavelengths. Placed between the sample and the spectrograph, the filter reflects radiation scattered at the Rayleigh wavelength while transmitting Stokes-shifted Raman scattering.

The transmission characteristics of these filters exhibit an angle dependence. With normal incidence, the filter has the highest OD at the design wavelength, but the Raman working window encompasses only bands that are Stokes-shifted by >650 cm^{-1} from the Rayleigh wavelength. However, with an increasing angle of incidence the bandpass working window is blue-shifted and encompasses bands that are Stokes-shifted by as little as 250 cm^{-1}. Thus, while maximum Rayleigh rejection is achieved with normal incidence, the filter can be angle-tuned to blue-shift the working window for the measurement of Raman bands close to the Rayleigh line. When one is examining highly scattering samples, this blue shift may result in a rising Rayleigh tail underlying the low wavenumber-shifted Raman bands and stray-light artifacts. Therefore, the Rayleigh scattering intensity and desired Raman spectral window must both be considered when selecting the optimum filter-operating angle.

Furthermore, with an off-normal incidence angle, these filters show a small but significant polarization dependence. Scattered radiation incident with *p*-polarization will be preferentially transmitted by the filter, especially at low wavenumber shifts from the Rayleigh wavelength. Thus when one is using the filters during the measurement of UVR-depolarization ratios, they should be used at normal incidence or positioned after the polarization scrambler.

The dielectric stack filters are stable in normal working environments. They exhibit no observable degradation following repeated temperature cycling to >500 K or through cycles of relative humidity from 0 to 100%. The bandpass shows a negligible and reversible red shift by ~20 cm^{-1} between 0 and 100% humidity, but more importantly, a significant blue shift is observed at high operating temperatures. This blue shifting of the bandpass toward the filter-design wavelength reduces Rayleigh rejection efficiency, thus limiting operation of the filters at high temperature.

We have utilized these dielectric stack filters in conjunction with a high-throughput single-stage spectrograph for UVR examinations. We have measured the 290-cm^{-1} UVR band of Teflon™, a highly scattering solid sample, with excitation wavelengths of 228.9 and 244 nm.

The high throughput of the filtered single-stage spectrograph enabled the measurement of high S/N resonance and preresonance Raman spectra from the photo-labile samples, including calf thymus DNA, PETN, and TNT, while using sufficiently low excitation powers and accumulation times to minimize photo-alteration.

These dielectric filters are readily incorporated within a UV optical-fiber Raman probe head to enable both the removal of background silica Raman signals and Rayleigh rejection. Using a 244-nm UV optical-fiber probe, we measured UVR spectra from 100 nM to mM concentrations of PAH in water and in an equimolar aqueous solution of the visible fluorophore R6G. Thus, we demonstrated the potential of UVR optical-fiber probes for minimally invasive, *in situ,* real-time monitoring of low analyte concentrations. In addition, we demonstrated that these *in situ* measurements could readily be made under conditions where fluorescence interference would prevent visible Raman optical-fiber probe measurements.

The sensitivity, selectivity, and immunity from fluorescence interference of UVRR combined with both the high efficiency of a Rayleigh-filtered single spectrograph and the sampling versatility of a filtered optical-fiber probe will enable numerous important analytical applications of UVR spectroscopy. Potential applications include remote monitoring of environmental pollutants, *in vivo* examination of biological systems, and real-time screening for contraband materials including controlled substances and energetic materials.

ACKNOWLEDGMENTS

We gratefully thank A. G. Mercado at the Federal Aviation Administration, NJ, for providing energetic material samples, and John F. Jackovitz at Westinghouse-Bettis, for his support of UV optical-fiber applications. We acknowledge support from an AFOSR Grant to the University of Pittsburgh Materials Research Center (F49620-95-1-0167) and from NIH Grant R01GM30741-14.

1. L. D. Ziegler and B. S. Hudson, J. Chem. Phys. **79,** 1134 (1983).
2. S. A. Asher and C. R. Johnson, Science **225,** 311 (1984).
3. S. A. Asher, C. R. Johnson, and J. Murtaugh, Rev. Sci. Instrum. **54,** 1657 (1983).
4. S. A. Asher, Anal. Chem. **56,** 720 (1984).
5. S. A. Asher, Anal. Chem. **56,** 2258 (1984).
6. W. L. Kubasek, B. Hudson, and W. Peticolas, Proc. Natl. Acad. Sci. USA **82,** 2369 (1985).
7. S. P. A. Fodor and T. G. Spiro, J. Am. Chem. Soc. **108,** 3198 (1986).
8. B. Hudson and L. Mayne, Methods Enzymol. **130,** 331 (1986).
9. C. R. Johnson, M. Ludwig, and S. A. Asher, J. Am. Chem. Soc. **108,** 905 (1986).
10. B. S. Hudson and L. C. Mayne, in *Biological Applications of Raman Spectroscopy,* T. G. Spiro, Ed. (John Wiley and Sons, New York, 1987), Vol. II.
11. S. A. Asher, Ann. Rev. Phys. Chem. **39,** 537 (1988).

12. R. Rumelfanger, S. A. Asher, and M. B. Perry, Appl. Spectrosc. **42,** 267 (1988).
13. C. M. Jones and S. A. Asher, J. Chem. Phys. **89,** 2649 (1988).
14. S. Song, S. A. Asher, S. Krimm, and J. Bandekar, J. Am. Chem. Soc. **110,** 8547 (1988).
15. M. Ludwig and S. A. Asher, J. Am. Chem. Soc. **110,** 1005 (1988).
16. R. J. Sension and B. S. Hudson, J. Chem. Phys. **90,** 1377 (1989).
17. J. Teraoka, P. A. Harmon, and S. A. Asher, J. Am. Chem. Soc. **112,** 2892 (1990).
18. P. A. Harmon, J. Teraoka, and S. A. Asher, J. Am. Chem. Soc. **112,** 8789 (1990).
19. T. G. Spiro, G. Smulevich, and C. Su, Biochemistry **29,** 4497 (1990).
20. P. A. Harmon, and S. A. Asher, J. Chem. Phys. **93,** 3064 (1990).
21. I. Harada, T. Yamagishi, K. Uchida, and H. Takeuchi, J. Am. Chem. Soc. **112,** 2443 (1990).
22. R. A. Copeland and T. G. Spiro, Biochemistry **29,** 4497 (1990).
23. J. D. Getty, S. D. Westre, D. Z. Bezebeh, G. A. Barral, M. J. Burmeister, and P. B. Kelly, Appl. Spectrosc. **46,** 620 (1992).
24. N. Cho and S. A. Asher, J. Am. Chem. Soc. **115,** 6349 (1993).
25. S. A. Asher, Anal Chem. **65,** 59A (1993).
26. S. A. Asher, Anal Chem. **65,** 201A (1993).
27. R. W. Bormett, S. A. Asher, R. E. Witkowski, W. D. Partlow, R. Lizewski, and F. Pettit, J. Appl. Phys. **77,** 5916 (1995).
28. S. A. Asher, R. W. Bormett, X. G. Chen, D. H. Lemmon, N. Cho, P. Peterson, M. Arrigoni, L. Spinelli, and J. Cannon, Appl. Spectrosc. **47,** 628 (1993).
29. J. S. W. Holtz, R. W. Bormett, Z. Chi, N. Cho, V. Pajcini, S. A. Asher, M. Arrogoni, P. Owen, and L. Spinelli, Appl. Spectrosc. **50,** 149 (1996)
30. C. H. Munro and S. A. Asher, Photonics Spectra **March,** 118 (1996).
31. C. Meyers, Princeton Instruments, Inc., personal communication.
32. M. M. Carrabba, K. M. Spencer, C. Rich, and D. Rauh. Appl. Spectrosc. **44,** 1558 (1990).
33. D. N. Batchelder and C. Cheng, U.S. Patent 05442438.
34. K. P. J. Williams, G. D. Pitt, B. J. E. Smith, A. Whitley, D. N. Batchelder, and I. P Hayward, J. Raman Spectrosc. **25,** 131 (1994).
35. T. P. Jannson, J. L. Jannson, and M. T. Feeney, U.S. Patent 05221957.
36. B. Yang, M. D. Morris, and H. Owens, Appl. Spectrosc. **45,** 1533 (1991).
37. P. L. Flaugh, S. E. O'Donnell, and S. A. Asher, Appl. Spectrosc. **38,** 847 (1984).
38. M. J. Pelletier, Appl. Spectrosc. **46,** 395 (1992).
39. M. J. Pelletier, Appl. Spectrosc. **47,** 69 (1993).
40. V. Pajcini, C. H. Munro, R. W. Bormett, R. E. Witkowski, and S. A. Asher, Appl. Spectrosc. **51,** 81 (1997).
41. T. Yanagimachi, H. Oguri, J. Nayyer, S. Ishihara, and J. Minowa, Appl. Optics **33,** 3513 (1994).
42. D. C. Blazej and W. L. Peticolas, Proc. Natl. Acad. Sci. USA **74,** 2639 (1977).
43. A. T. Tu, *Raman Spectroscopy in Biology* (Wiley, New York, 1982).
44. M. Majoube, P. Millie, P. Lagant, and G. Vergoten, J. Raman Spectrosc. **25,** 821 (1994).
45. M. M. Carrabba, J. Haas III, J. Bello, and R. Forney, Proc. Pittcon '96 1004 (1996).
46. T. F. Cooney, H. T. Skinner, and S. M. Angel, Appl. Spectrosc. **50,** 3513 (1996).
47. P. J. Hendra, G. Ellis, and D. J. Cutter, J. Raman Spectrosc. **19,** 413 (1988).
48. H. Yamada and Y. Yamamoto, J. Raman Spectrosc. **9,** 401 (1980).
49. S. D. Schwab, R. McCreery, and F. T. Gamble, Anal. Chem. **58,** 2486 (1986).
50. I. P. Hayward, T. E. Kirkbride, D. N. Batchelder, and R. J. Lacey, J. For. Sci. **40,** 883 (1995).
51. M. M. Carrabba and R. D. Rauh, U.S. Patent 05112127.
52. H. Owen, J. M. Tedesco, and J. B. Slater, U.S. Patent 05377004.
53. S. M. Angel, T. F. Cooney, and H. T. Skinner, in *Proceedings of the Fifteenth International Conference on Raman Spectroscopy,* S. A. Asher and P. B. Stein, Eds. (John Wiley and Sons, Chichester, United Kingdom, 1996), p. 1078.
54. K. W. Jennette, A. M. Jeffrey, S. H. Blobstein, F. A. Beland, R. G. Harvey, and I. B. Weinstein, Biochemistry **16,** 932 (1977).
55. R. G. Harvey, in *Proceedings of the Working Group on Molecular Mechanisms of Carcinogenic and Antitumor Activity,* Pontificiae Academiae Scientairum Scripta Varia Vol. **70,** C. Chagas and B. Pullman, Eds. (Adenine Press, New York, 1986), p. 95.
56. N. E. Geacintov, H Yoshida, V. Ibanez, and R. G. Harvey, Biochem. Biophys. Res. Comm. **100,** 1569 (1981).
57. Z. Chi and S. A. Asher, in *Proceedings of the Fifteenth International Conference on Raman Spectroscopy,* S. A. Asher and P. B. Stein, Eds. (John Wiley and Sons, Chichester, 1996), p. 1112.